Inorg. Chem. **2002**, *41*, 3102–3109

Structural, Spectroscopic, and Reactivity Comparison of Xanthene- and Dibenzofuran-Bridged Cofacial Bisporphyrins

Christopher J. Chang, Erin A. Baker, Bradford J. Pistorio, Yongqi Deng, Zhi-Heng Loh, Scott E. Miller, Scott D. Carpenter, and Daniel G. Nocera*

Department of Chemistry, 6-335, Massachusetts Institute of Technology, 77 Massachusetts Avenue, Cambridge, Massachusetts 02139

Received October 23, 2001

A comparison of the structure, spectroscopy, and oxygen atom-transfer reactivity of cofacial bisporphyrins anchored by xanthene (DPX) and dibenzofuran (DPD) pillars is presented. The synthesis and characterization of dicopper(II) and dinickel(II) complexes of DPD completes a homologous series of homobimetallic zinc(II), copper(II), and nickel(II) complexes for both cofacial platforms. X-ray crystallographic analysis of the parent free-base porphyrins H_4DPX (**1**) and H_4DPD (**5**) confirms the face-to-face arrangement of the two porphyrin macrocycles with a large available range of vertical pocket sizes: **1** ($C_{80}H_{92}Cl_2N_8O$), triclinic, space group $P\bar{1}$, $a = 13.5167(12)$ Å, $b = 21.7008(18)$ Å, $c = 23.808(2)$ Å, $\alpha = 80.116(2)°$, $\beta = 76.832(2)°$, $\gamma = 80.4070(10)°$, $Z = 4$; **5** ($C_{80}H_{83}N_8O_2$), monoclinic, space group $C2/c$, $a = 22.666(2)$ Å, $b = 13.6749(14)$ Å, $c = 42.084(4)$ Å, $\beta = 94.554(2)°$, $Z = 8$. EPR spectroscopy of dicopper(II) derivatives Cu_2DPX (**3**) and Cu_2DPD (**7**) complements the crystallographic studies by probing intramolecular metal–metal arrangements in frozen solution. Exciton interactions between the porphyrin subunits in fluid solution are revealed by steady-state and time-resolved electronic absorption and emission spectroscopy. The resulting compilation of structural and spectroscopic data provides a benchmark for the use of these and related platforms for the activation of small-molecule substrates. A structure–function relation is developed for the photoinduced oxygen atom-transfer reactions of bisiron(III) μ-oxo derivatives of DPX and DPD. The efficiency of the photochemical process is markedly dependent ($\sim 10^4$-fold) on the vertical flexibility of cofacial architecture provided by the spacer.

Introduction

Ongoing investigations of cofacial bisporphyrins are motivated by their utility for the binding and multielectron activation of small-molecule substrates within the clefts of these compounds.[1] Over the past 25 years, the singly bridged "Pacman" systems have featured two spacers, anthracene (DPA) and biphenylene (DPB).[1−14] The exceptional activity of DPA and DPB cofacial bisporphyrins is based on their ability to impair *lateral* slippage between porphyrin rings, thus allowing for efficient multielectron small-molecule transformations with little structural reorganization of jux-

* Author to whom correspondence should be addressed. E-mail: nocera@mit.edu.

(1) Collman, J. P.; Wagenknecht, P. S.; Hutchinson, J. E. *Angew. Chem., Int. Ed. Engl.* **1994**, *33*, 1537−1554.
(2) Chang, C. K.; Abdalalmuhdi, I. *J. Org. Chem.* **1983**, *48*, 5388−5390.
(3) Chang, C. K.; Abdalmuhdi, I. *Angew. Chem., Int. Ed. Engl.* **1984**, *23*, 164−165.
(4) Chang, C. K.; Liu, H. Y.; Abdalmuhdi, I. *J. Am. Chem. Soc.* **1984**, *106*, 2725−2726.
(5) Collman, J. P.; Hutchinson, J. E.; Lopez, M. A.; Tabard, A.; Guilard, R.; Seok, W. K.; Ibers, J. A.; L'Her, M. *J. Am. Chem. Soc.* **1992**, *114*, 9869−9877.
(6) Collman, J. P.; Hutchinson, J. E.; Ennis, M. S.; Lopez, M. A.; Guilard, R. *J. Am. Chem. Soc.* **1992**, *114*, 8074−8080.
(7) Fillers, J. P.; Ravichandran, K. G.; Abdalmuhdi, I.; Tulinsky, A.; Chang, C. K. *J. Am. Chem. Soc.* **1986**, *108*, 417−424.
(8) Guilard, R.; Lopez, M. A.; Tabard, A.; Richard, P.; Lecomte, C.; Brandes, S.; Hutchinson, J. E.; Collman, J. P. *J. Am. Chem. Soc.* **1992**, *114*, 9877−9889.
(9) Guilard, R.; Brandes, S.; Tardieux, C.; Tabard, A.; L'Her, M.; Miry, C.; Gouerac, P.; Knop, Y.; Collman, J. P. *J. Am. Chem. Soc.* **1995**, *117*, 11721−11729.
(10) Harvey, P. D.; Proulx, N.; Martin, G.; Drouin, M.; Nurco, D. J.; Smith, K. M.; Bolze, F.; Gros, C. P.; Guilard, R. *Inorg. Chem.* **2001**, *40*, 4134−4142.
(11) Le Mest, Y.; Inisan, C.; Laouenan, A.; L'Her, M.; Talarmain, J.; El Khalifa, M.; Saillard, J. Y. *J. Am. Chem. Soc.* **1997**, *119*, 6905−6106.
(12) Lui, H.-Y.; Abdalmuhdi, I.; Chang, C. K.; Anson, F. C. *J. Phys. Chem.* **1985**, *89*, 665−670.
(13) Ni, C.-L.; Abdalmuhdi, I.; Chang, C. K.; Anson, F. C. *J. Phys. Chem.* **1987**, *91*, 1158−1166.
(14) Naruta, Y.; Sasayama, M.; Ichihara, K. *J. Mol. Catal. A* **1997**, *117*, 115−121.

10.1021/ic0111029 CCC: $22.00
Published on Web 05/16/2002

Chart 1

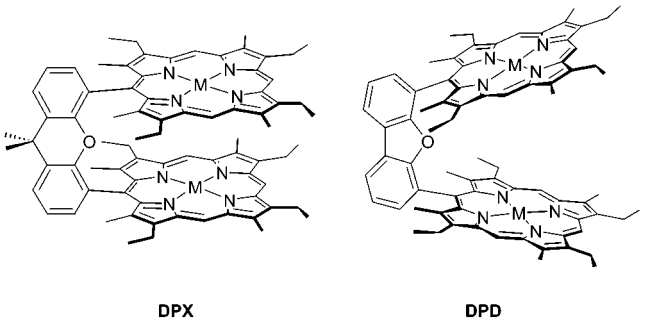

taposed subunits. We became interested in testing the structural limits of *vertical* flexibility within the Pacman motif in order to expand the use of such platforms for multielectron catalysis.[15] For the DPA and DPB scaffolds, a difference in the vertical pocket size of ca. 1 Å offers a limited range of conformational flexibility for examining structure−reactivity relationships derived from the Pacman effect. With the goal of increasing the span of the Pacman bite, we recently introduced two novel cofacial bisporphyrins bearing the cyclic ether spacers xanthene (DPX)[16] and dibenzofuran (DPD).[17] The DPX and DPD systems of Chart 1 afford an unprecedented range of vertical pocket sizes while maintaining a face-to-face arrangement of porphyrin subunits. In particular, the DPD platform has provided direct structural evidence for the Pacman effect within a single pillared cofacial bisporphyrin motif.[17] A comparative structural analysis of bizinc(II) and bisiron(III) μ-oxo complexes of DPD has shown the unique ability of this platform to open and close its binding pocket by a vertical distance of over 4 Å.

To understand the effects of pocket size and flexibility on the multielectron reactivity of pillared cofacial bisporphyrins, we report here a systematic structural and spectroscopic study of the DPX and DPD platforms using a homologous set of homobimetallic zinc(II), copper(II), and nickel(II) complexes; the compiled data in this report provide a useful benchmark for comparing and contrasting cofacial bisporphyrin systems with large differences in vertical tunability and flexibility. In addition, these results are augmented by a comparative reactivity study; specifically, we have investigated the consequences of the Pacman effect on the multielectron reactivity of the cofacial bisporphyrin systems by examining the photoinduced oxygen atom-transfer reactivity of bisiron(III) μ-oxo derivatives of DPX and DPD with phosphite substrates. Our findings reveal that a remarkably enhanced efficiency (by ca. 4 orders of magnitude) for this multielectron photooxidation process is a direct consequence of the unique ability of the DPD platform to undergo large, facile changes in vertical cleft size by the Pacman effect.

(15) Chang, C. J.; Brown, J. D. K.; Chang, M. C. Y.; Baker, E. A.; Nocera, D. G. In *Electron Transfer in Chemistry*; Balzani, V., Ed.; Wiley-VCH: Weinheim, Germany, 2001; Vol. 3.2.4, pp 409−461.

(16) Chang, C. J.; Deng, Y.; Heyduk, A. F.; Chang, C. K.; Nocera, D. G. *Inorg. Chem.* **2000**, *39*, 959−966.

(17) Deng, Y.; Chang, C. J.; Nocera, D. G. *J. Am. Chem. Soc.* **2000**, *122*, 410−411.

Experimental Section

Materials. Silica gel 60 (70−230 and 230−400 mesh, Merck) was used for column chromatography. Analytical thin-layer chromatography was performed using Merck 60 F254 silica gel (precoated sheets, 0.2 mm thick). Solvents for synthesis were of reagent grade or better and were dried according to standard methods.[18] Spectroscopic experiments employed dichloromethane (spectroscopic grade, Burdick & Jackson), which was stored over 4-Å molecular sieves under high vacuum or in a glovebox. Cofacial bisporphyrins H_4(DPX) (**1**), Zn_2(DPX) (**2**), Cu_2(DPX) (**3**), Ni_2(DPX) (**4**), H_4(DPD) (**5**), Zn_2(DPD) (**6**), and Fe_2O(DPD) (**10**) were prepared as previously described.[16,17] All other reagents were used as received. Mass spectral analyses were carried out by the University of Illinois Mass Spectrometry Laboratory. Elemental analyses were performed at H. Kolbe Mikroanalytisches Laboratorium and Quantitative Technologies, Inc.

Cu_2(DPD) (7). To a 20-mL chloroform solution of **5** (50 mg, 0.045 mmol) was added a solution of $Cu(OAc)_2 \cdot 2H_2O$ (100 mg) and potassium acetate (110 mg) in 15 mL of methanol. The resulting solution was refluxed for 4 h and solvent was removed by rotary evaporation. The solid was taken up in a 1:1 mixture of dichloromethane/water (40 mL). The organic layer was decanted, washed with water (3 × 15 mL), dried over Na_2SO_4, and taken to dryness. The crude material was purified by flash column chromatography (silica gel, 3:1 dichloromethane/hexanes), followed by recrystallization from dichloromethane/methanol to afford analytically pure **7** as a cherry red solid (50 mg, 90% yield). Anal. Calcd for $C_{76}H_{76}N_8OCu_2 \cdot H_2O$: C, 72.30; H, 6.23; N, 8.88. Found: C, 72.49; H, 6.10; N, 8.78. HRFABMS (M^+) calcd for $C_{79}H_{82}N_8OCu_2$ *m*/*z* 1243.481, found 1243.481.

Ni_2(DPD) (8). A mixture of **5** (53 mg, 0.047 mmol) and $NiCl_2$ (110 mg) in 15 mL of DMF was refluxed for 5 h. The solvent was removed under vacuum and the remaining solid was taken up in a 1:1 mixture of dichloromethane/water (100 mL). The organic layer was decanted, washed with water (3 × 50 mL), dried over Na_2SO_4, and taken to dryness. Purification by flash column chromatography (silica gel, 3:1 dichloromethane/hexanes) followed by recrystallization from dichloromethane/methanol gave analytically pure **8** as a plum red solid (48 mg, 82% yield). ^{1}H NMR (500 MHz, $CDCl_3$, 25 °C): δ = 9.33 (s, 4H, meso), 9.32 (s, 2H, meso), 8.51 (d, 2H, ArH), 7.62 (t, 2H, ArH), 7.27 (d, 2H, ArH), 3.68 (m, 16H, CH_2), 3.25 (s, 12H, CH_3), 2.32 (s, 12H, CH_3), 1.58 (t, 12H, CH_3), 1.51 (t, 12H, CH_3). Anal. Calcd for $C_{76}H_{76}N_8ONi_2$: C, 73.92; H, 6.20; N, 9.07. Found: C, 74.15; H, 6.35; N, 8.68. HRFABMS (M^+) calcd for $C_{76}H_{76}N_8ONi_2$ *m*/*z* 1232.485, found 1232.492.

Fe_2O(DPX) (9). In a drybox, **1** (20 mg, 0.017 mmol), pyridine (0.1 mL), $FeBr_2$ (60 mg), and THF (15 mL) were loaded in a 50-mL flask equipped with a condenser. The mixture was refluxed under nitrogen for 5 h, opened to air, and brought to dryness under vacuum. The residue was purified using basic alumina (activity I, chloroform/ethyl acetate = 80/20) to give **9** as a brown solid (18 mg, 90% yield). Anal. Calcd for $C_{79}H_{82}Fe_2N_8O_2$: C, 73.71; H, 6.42, N, 8.70, Found: C, 73.77, H, 6.31, N, 8.68. HRFABMS ($M - O^+$) calcd for $C_{79}H_{82}Fe_2N_8O_2$ *m*/*z*, 1270.5310, found 1270.5316.

General Details of X-ray Data Collection and Reduction. X-ray diffraction data were collected using a Siemens 3 circle diffractometer equipped with a CCD detector. Measurements were carried out at −90 °C using Mo Kα (λ = 0.71073 Å) radiation, which was wavelength selected with a single-crystal graphite monochromator. Four sets of data were collected using ω scans

(18) Armarego, W. L. F.; Perrin, D. D. *Purification of Laboratory Chemicals*, 4th ed.; Butterworth-Heinmann: Oxford, 1996.

and a −0.3° scan width. All calculations were performed using a PC workstation. The data frames were integrated to *hkl*/intensity, and final unit cells were calculated by using the SAINT v.4.050 program from Siemens. The structures were solved and refined with the SHELXTL v.5.03 suite of programs developed by G. M. Sheldrick and Siemens Industrial Automation, Inc., 1995.

X-ray Structure of H_4(DPX) (1). A 0.52 mm × 0.24 mm × 0.10 mm purple red crystal of plate morphology was obtained from slow evaporation of a methanol/dichloromethane solution of the compound. The crystal was coated in Paratone N and mounted onto a glass fiber. A total of 18 992 reflections were collected in the θ range 2.25° to 20.00°, of which 12 281 were unique ($R_{int} = 0.0342$). Hydrogen atoms were placed in calculated positions using a standard riding model and were refined isotropically. The largest peak and hole in the difference map were 0.395 and −0.703 e Å^{-3}, respectively. The least-squares refinement converged normally, giving residuals of R1 = 0.0552 and wR2 = 0.1494, with GOF = 1.029. Crystal data for $C_{80}H_{92}Cl_2N_8O$: triclinic, $P\bar{1}$, $Z = 4$, a = 13.5167(12) Å, b = 21.7008(18) Å, c = 23.808(2) Å, α = 80.116(2)°, β = 76.832(2)°, γ = 80.4070(10)°, V = 6639.4(10) Å^3, ρ_{calc} = 1.253 g/cm^3, $F(000) = 2680$.

X-ray Structure of H_4(DPD) (5). A 0.35 mm × 0.20 mm × 0.20 mm brick red crystal of block morphology was obtained from vapor diffusion of pentane into an acetone solution of the compound. The crystal was coated in STP and mounted onto a glass fiber. A total of 25 700 reflections were collected in the θ range 2.32° to 23.29°, of which 9347 were unique ($R_{int} = 0.0534$). Hydrogen atoms bound to nitrogen in the porphyrin ring were located, and their positions were stable. Other hydrogen atoms were placed in calculated positions using a standard riding model and were refined isotropically. The largest peak and hole in the difference map were 1.036 and −0.358 e Å^{-3}, respectively. The least squares refinement converged normally, giving residuals of R1 = 0.0763 and wR2 = 0.1708, with GOF = 1.148. Crystal data for $C_{80}H_{83}N_8O_2$: monoclinic, $C2/c$, $Z = 8$, a = 22.666(2) Å, b = 13.6749(14) Å, c = 42.084(4) Å, β = 94.554(2)°, V = 13003(2) Å^3, ρ_{calc} = 1.214 g/cm^3, $F(000) = 5080$.

Physical Measurements. ^{1}H NMR and ^{31}P NMR spectra were collected in $CDCl_3$ (Cambridge Isotope Laboratories) at 25 °C in the MIT Department of Chemistry Instrumentation Facility (DCIF) using a Unity 300, a Mercury 300, or an Inova 500 spectrometer. All chemical shifts are reported using the standard δ notation in parts-per-million; positive chemical shifts are to higher frequency from the given reference. X-band EPR spectra were recorded in toluene glass (between 120 and 160 K) in 4-mm quartz tubes using a Bruker 300 EMX EPR spectrometer. Data were analyzed using the Win-EPR program. Absorption spectra were obtained using a Cary-17 spectrophotometer modified by On-Line Instrument Systems (OLIS) to include computer control or a Spectral Instruments 440 Model spectrophotometer.

Samples for all photochemical and photophysical measurements were contained within a cell equipped with a solvent reservoir and a 1-cm clear fused-quartz cell (Starna Cells, Inc.). The two chambers were isolated from each other by a high-vacuum Teflon valve and from the environment by a second high-vacuum Teflon valve. Samples were subject to at least three freeze−pump−thaw cycles (10^{-6} Torr). Emission spectra were recorded using a high-resolution instrument described previously.[19] Integrated emission fluorescence quantum yields (Φ_{fl}) were determined relative to Zn(TPP) (TPP = 5,10,15,20-tetraphenylporphyrin) as a standard (Φ_{fl} = 0.04 in methylcyclohexane). Luminescence lifetime measurements were carried out using a Hamamatsu C4334-0 Streak Camera. Excitation pulses (95 μJ, 400 nm) were generated from the second harmonic of a commercial 1-kHz Ti:sapphire based chirped pulse regenerative amplifier system described in a previous report.[16] Bulk photolyses were performed on stirred solutions contained in a quartz reaction vessel adapted for manipulations on a high-vacuum manifold. Samples were irradiated at 25 °C using a 1000-W high-pressure Oriel Hg−Xe lamp. The irradiation beam passed through cutoff filters to remove high-energy light and a collimating lens prior to entering the sample chamber. Quantum yield experiments were performed by replacing the cutoff filters with 10-nm band-pass mercury line interference filters (Oriel). The standard ferrioxalate technique was employed for the calculation of product quantum yields.[20] Photolysis reactions were monitored by using absorption spectroscopy.

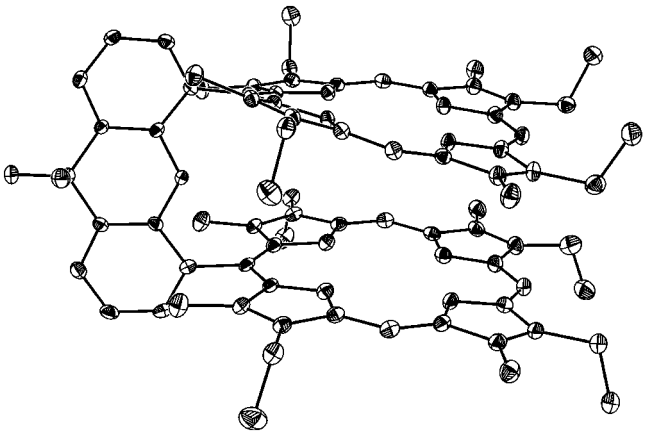

Figure 1. Crystal structure of H_4(DPX) (**1**). Thermal ellipsoids are drawn at the 25% probability level. Hydrogen atoms have been omitted for clarity.

Results and Discussion

Synthesis. Homobimetallic complexes of H_4(DPD) (**5**) are readily produced by reaction with metal salts. For example, treatment of **5** with $Cu(OAc)_2 \cdot 2H_2O$ in methanol/chloroform mixtures affords the corresponding binuclear copper(II) complex Cu_2(DPD) (**7**) in excellent yield (90%). Complex **7** gave satisfactory mass spectral and elemental analyses. Also, Ni_2(DPD) (**8**) was prepared according to Adler's method ($NiCl_2$/refluxing DMF) in good yield (82%). The diamagnetic complex was characterized using ^{1}H NMR, high-resolution mass spectrometry, and elemental analyses. The successful preparation of **7** and **8** completes a series of structurally homologous cofacial bisporphyrin complexes for DPX and DPD containing zinc(II), copper(II), and nickel(II).

Structural Comparison. The molecular structures of **1** and **5**, shown in Figures 1 and 2, respectively, offer a direct structural comparison between DPX and DPD congeners. Each atom of the porphyrin rings and the corresponding bridge is numbered in the standard convention (see Supporting Information), while auxiliary methyl and ethyl groups off the macrocycles are additionally identified according to their point of attachment to the porphyrin ring. Crystallographic data are given in Table 1, and selected geometrical

(19) Rudzinski, C. M.; Engebretson, D. S.; Hartmann, W. K.; Nocera, D. G. *J. Phys. Chem. A* **1998**, *102*, 7442−7446.

(20) Murov, S. L.; Carmichael, I.; Hug, G. L. *Handbook of Photochemistry*; 2nd ed.; Marcel Dekker: New York, 1993.

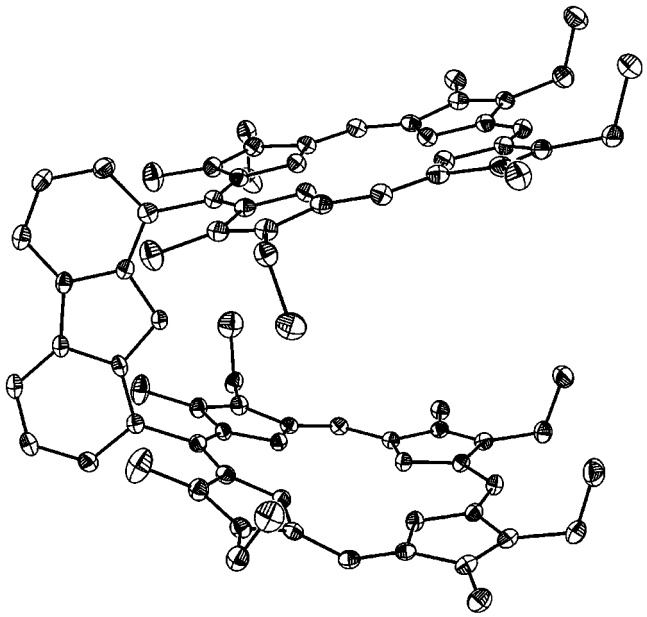

Figure 2. Crystal structure of H_4(DPD) (**5**). Thermal ellipsoids are drawn at the 25% probability level. Hydrogen atoms have been omitted for clarity.

Table 1. Crystallographic Data for **1** and **5**

	1	**5**
empirical formula	$C_{79}H_{82}N_8O$	$C_{80}H_{83}N_8O_2$
fw	1252.52	1188.54
T (K)	183(2)	183(2)
λ (Å)	0.71073	0.71073
crystal system	triclinic	monoclinic
space group	$P\bar{1}$	$C2/c$
a (Å)	13.5167(12)	22.6650(2)
b (Å)	21.7008(18)	13.6749(14)
c (Å)	23.8080(2)	42.0840(4)
α (deg)	80.1160(2)	90
β (deg)	76.8320(2)	94.5540(2)
γ (deg)	80.4070(10)	90
V (Å^3)	6639.40(10)	13 003(2)
Z	4	8
ρ_{calcd} (g cm^{-3})	1.253	1.146
abs coeff (mm^{-1})	0.152	0.068
F(000)	2680	4800
no. of reflns collcd	18 992	25 700
(R_{int}) ind reflns	12 281(0.0342)	9347 (0.0473)
max/min transm	0.5987/0.9630	0.4975/0.6515
data/restraints/params	12 281/0/1676	9347/0/874
R1,[a] wR2[b]	0.0552, 0.1494	0.0765, 0.1727
R1,[a] wR2[b](all data)	0.0715, 0.1588	0.0980, 0.1816
GOF[c] on F^2	1.029	1.172
extinction coeff	0.0012(17)	none used

[a] $R1 = \sum||F_o| - |F_c||/\sum|F_o|$. [b] $wR2 = (\sum(w(F_o^2 - F_c^2)^2)/\sum(w(F_o^2)^2))^{1/2}$. [c] $GOF = (\sum w(F_o^2 - F_c^2)^2/(n - p))^{1/2}$, where n is the number of data and p is the number of parameters refined.

measurements are given in Tables 2 and 3. Trends in bond lengths and angles of macrocyclic core structures and side chains agree well with those observed in related cofacial bisporphyrins.[1,5,7−9,16,17] Specific features of the core structures for **1** and **5** are highlighted below:

H_4(DPX) (1). A conformational analysis of the two macrocycles reveals inequivalent ring systems. The macrocycle containing N(1) to N(4) (see Supporting Information for atom numbering scheme) exhibits a slightly ruffled S_4 conformation, with a mean deviation from planarity of 0.2885 Å. In contrast, the macrocycle containing N(5) to N(8) displays a saddle conformation with a mean deviation from planarity of 0.3548 Å. A similar ring inequivalence effect has been observed in a number of pillared bisporphyrin systems and has been attributed to a localized macrocyclic distortion induced by the steric crowding of a large meso substituent flanked by proximate alkyl groups.[21] The hydrogen atoms inside the porphyrin rings are in their calculated positions and are disordered over all nitrogen atoms. Lastly, a notable feature concerning the structure of free-base **1** is the severe butterfly fold of the xanthene backbone along its center O(1)−C(47) axis. This bent distortion is best described in terms of an intraplanar angle through the center axis fold. For **1**, the butterfly angle is 36.1°. In contrast, metal derivatives of DPX typically display a flattened spacer with butterfly angles in the range of 6°−15° [Zn(II), 15.2°; Cu(II), 14.1°; Ni(II), 6.4; Co(II), 6.2], with smaller metal cations causing a greater distortion of the bridge from its naturally bent fold.[16,22]

H_4(DPD) (5). As observed for **1**, the two ring systems of **5** are structurally inequivalent in the solid state; however, unlike **1**, both porphyrin subunits of **5** display a ruffled S_4 conformation. The macrocycle with N(1) to N(4) is nearly planar, with a mean deviation of 0.0553 Å for the macrocyclic atoms from the porphyrin mean plane. The meso carbons are alternately displaced from the mean porphyrin plane, ranging from 0.0758 Å above to 0.0822 Å below the 24-atom macrocyclic unit. The macrocycle containing N(5) to N(8) has a more pronounced ruffled structure. The mean deviation of 0.1639 Å from the porphyrin plane is greater than that observed in the ring containing N(1) to N(4), and the meso carbons are displaced from 0.3121 Å below to 0.3938 Å above the mean porphyrin plane. An acetone molecule modeled at 50% occupancy over two sites was located in the DPD pocket. Although the lengths of the two overlapping carbon−carbon bonds are longer than expected for acetone, the model was stable throughout the refinement. The hydrogen atoms inside the ring were located from the electron difference map, and their positions were also stable over the course of refinement.

The structures of the parent free-base bisporphyrins add to the rapidly growing body of structural data for the DPX and DPD systems. The three mutually perpendicular views of the molecular structures of **1** and **5** shown in Figure 3 confirm the ability of the xanthene and dibenzofuran bridges to confine the two porphyrin rings to a face-to-face arrangement while producing molecular clefts with a wide range of vertical pocket sizes. Pertinent geometrical intradimer features for DPX and DPD complexes characterized by X-ray crystallography are summarized in Table 3.[23,24] Definitions for geometric measurements are given in Table 3 and Figure 4. The collected data illustrate the significant effect of substituting a single six-membered ether ring (DPX) for a

(21) Clement, T. E.; Nurco, D. J.; Smith, K. M. *Inorg. Chem.* **1998**, *37*, 1150−1160.
(22) Chang, C. J.; Deng, Y.; Shi, C.; Chang, C. K.; Anson, F. C.; Nocera, D. G. *Chem. Commun.* **2000**, 1355−1356.
(23) Scheidt, W. R.; Lee, Y. J. *Struct. Bonding (Berlin)* **1987**, *64*, 1−70.
(24) Scheidt, W. R.; Mondal, J. U.; Eigenbrot, C. W.; Adler, A.; Radonovich, L. J.; Hoard, J. L. *Inorg. Chem.* **1986**, *25*, 795−799.

Table 2. Selected Geometric Lengths (Å) and Angles (deg) Calculated for Compounds **1** and **5**

1				**5**			
Bond Distances/Å							
Ct(1)−N(1)	2.070	Ct(2)−N(5)	2.098	Ct(1)−N(1)	2.120	Ct(2)−N(5)	2.107
Ct(1)−N(2)	2.106	Ct(2)−N(6)	2.050	Ct(1)−N(2)	2.029	Ct(2)−N(6)	2.019
Ct(1)−N(3)	2.067	Ct(2)−N(7)	2.110	Ct(1)−N(3)	2.127	Ct(2)−N(7)	2.123
Ct(1)−N(4)	2.109	Ct(2)−N(8)	2.047	Ct(1)−N(4)	2.033	Ct(2)−N(8)	2.006
Bond Angles/deg							
N(1)−Ct(1)−N(2)	88.4	N(7)−Ct(2)−N(8)	88.6	N(1)−Ct(1)−N(2)	85.3	N(7)−Ct(2)−N(8)	85.5
N(1)−Ct(1)−N(3)	177.5	N(7)−Ct(2)−N(6)	91.9	N(1)−Ct(1)−N(3)	178.5	N(7)−Ct(2)−N(6)	94.9
N(2)−Ct(1)−N(3)	91.6	N(8)−Ct(2)−N(6)	179.0	N(2)−Ct(1)−N(3)	94.6	N(8)−Ct(2)−N(6)	176.7
N(1)−Ct(1)−N(4)	91.5	N(7)−Ct(2)−N(5)	176.1	N(1)−Ct(1)−N(4)	94.8	N(7)−Ct(2)−N(5)	176.8
N(2)−Ct(1)−N(4)	179.5	N(8)−Ct(2)−N(5)	91.1	N(2)−Ct(1)−N(4)	178.5	N(8)−Ct(2)−N(5)	94.6
N(3)−Ct(1)−N(4)	88.3	N(6)−Ct(2)−N(5)	88.2	N(3)−Ct(1)−N(4)	85.3	N(6)−Ct(2)−N(5)	85.2

Table 3. Crystallographically Derived Intradimer Geometrical Features for DPX and DPD Compounds[a]

	M−M (Å)	Ct−Ct (Å)	MPS (Å)	interplanar angle (deg)	torsional twist (deg)	a−b dist (Å)	c−d dist (Å)
H_4(DPX) (**1**)	na	4.002	3.609	4.7	14.3	3.552	4.324
Zn_2(DPX) (**2**)	3.708	3.863	3.417	4.4	7.9	4.619	4.272
Cu_2(DPX) (**3**)	3.910	3.978	3.611	2.3	7.4	4.594	4.321
Ni_2(DPX) (**4**)	4.689	4.698	3.666	1.9	22.2	4.657	4.466
Co_2(DPX)	4.582	4.630	3.519	2.5	21.1	3.591	4.403
H_4(DPD) (**5**)	na	8.220	8.220	23.0	1.9	4.853	5.654
Zn_2(DPD) (**6**)	7.775	7.587	7.356	24.6	1.2	4.800	5.577
Co_2(DPD)·2MeOH	8.624	8.874	8.794	56.5	9.3	4.826	5.730
Fe_2O(DPD) (**10**)	3.504	4.611	4.871	21.1	1.9	4.763	5.082

[a] Metrics were derived as follows. Macrocyclic centers (Ct) were calculated as the centers of the four nitrogen planes (4-N plane) for each macrocycle. Interplanar angles were measured as the angle between the 4-N least squares planes. Plane separations were measured as the perpendicular distance from one macrocycle's 4-N least-squares plane to the center of the other macrocycle; mean plane separations (MPS) were the average of the two plane separations. Torsional twists were measured as the angle between the two meso-carbon to spacer bonds. The a−b and c−d distances were obtained according to the convention shown in Figure 4.

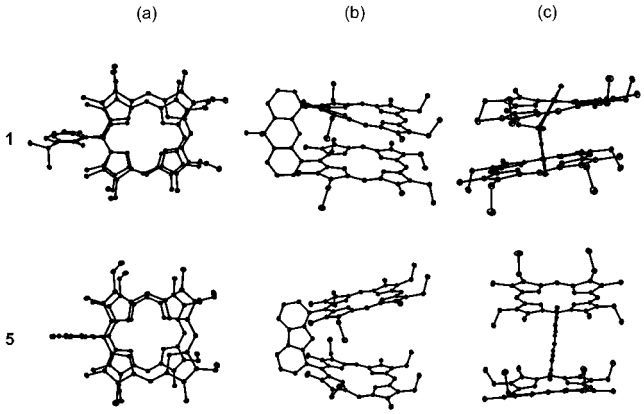

Figure 3. Comparative views of the crystal structures of **1** and **5**: (a) top view, normal to porphyrin planes; (b) side view, perpendicular to the bridge plane; (c) side view, along the bridge plane. Hydrogen atoms have been omitted for clarity.

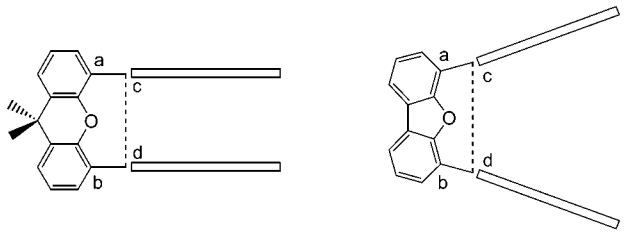

Figure 4. Illustrated distances a−b and c−d for the cofacial bisporphyrin systems DPX (left) and DPD (right). The footnote to Table 3 defines the methods by which the crystallographically derived geometric features were measured.

five-membered one (DPD). For example, in the absence of axial ligands, the center-to-center distances vary from 3.8 to 4.7 Å for the DPX platforms to 7.6 to 8.2 Å for the DPD compounds. The vertical range of almost 4 Å observed for DPX and DPD is in stark contrast to those of DPA and DPB, which differ by only ca. 1 Å in vertical size. Even more notable is the significant range of interplanar angles between the two macrocyclic subunits. The ring-parallel DPX complexes exhibit interplanar angles of less than 5°, while their ring-splayed DPD congeners display angles between 20° and 25°, all without the influence of axial ligands. For comparison, the corresponding values for unligated DPA and DPB complexes lie between 2° and 7°.[1,7] Lastly, the cofacial geometry of DPX and DPD is displayed by their small torsional angles, which are all less than 25°. The DPD complexes are especially noteworthy in this regard, with torsion angles of less than 10° in all cases.

A number of structural features can be used to tune the critical metal−metal distances, not the least of which is axial ligation. This is especially evident for DPD, where extremely compressed or splayed geometries can be achieved by the addition of axial ligands. With external ligation, the metal−metal distances of DPD can range from 3.504 Å, as found for Fe_2O(DPD) (**10**), which clamps its Pacman bite around a bridging oxo ligand, to 8.624 Å for Co_2(DPD), which coordinates two methanol solvates within its cofacial pocket. More subtle structural changes are available through metal substitution, which can influence the π overlap between porphyrin subunits. Within the DPX series, Ni_2(DPX) (**4**) and Co_2(DPX) exhibit the least π overlap, giving the largest torsional twists (ca. 20°) and metal−metal separations (ca. 4.6 Å) in the absence of any external axial ligands.

Table 4. Comparison of Geometric Intradimer Parameters Derived from EPR and X-ray Crystallography for Dicopper(II) Cofacial Bisporphyrins

	r_{exp} (Å)[a]	r_{sim} (Å)[b]	M−M (Å)[c]	interplanar (Å)[d]	MPS (Å)[c]
Cu_2(DPX) (**3**)	4.00	4.20	3.90	4.00	3.60
Cu_2(DPD) (**7**)	7.80	8.00		7.30	
Cu_2(DPA)	4.90	4.90	4.57	4.60	3.90
Cu_2(DPB)	4.14	4.13	3.81	3.90	3.50
Cu_2(FTF-4)	4.04	4.15		4.00	
Cu_2(FTF-5)	4.12	4.15		3.90	
Cu_2(FTF-7)	5.00	4.95	5.22	3.80	3.52
Cu_2(slip-4)	5.70	5.50		3.90	

[a] Determined from the ratio of the intensities of the half-field to allowed EPR transitions. [b] Estimated from dipolar splitting simulations. [c] From X-ray crystal structures. See the text for appropriate references. [d] Interplanar distances determined from EPR simulation.

The EPR spectra of homobimetallic copper(II) derivatives **3** and **7** in frozen solution provide a useful complement to crystallographic studies. Previous studies by Eaton et al. have demonstrated the validity of such methods for structure determination of related cofacial bisporphyrins.[25] The interspin geometry of the two paramagnetic Cu(II) centers can be obtained by examining their triplet spectrum, and the interspin distance, *r*, can be determined from the ratio of the intensity of the half-field transitions to the intensity of the allowed transitions. The dipolar splitting of both the copper parallel and perpendicular lines in **3** and **7** is clearly resolved with no evidence of aggregation. Simulation gives *r* values of 4.2 and 8.0 Å for **3** and **7**, respectively. The separations between the copper parallel lines (2D values) give Cu−Cu distances that agree with those obtained from the dipolar splitting simulations. The spectra of the half-field transitions of **3** and **7** provide another estimate of metal−metal separation. The ratio of the intensity of the half-field transitions to the intensity of the allowed transitions are 4.8×10^{-3} for **3** and 8.7×10^{-5} for **7**, giving interspin distances of 4.0 and 7.8 Å, respectively. The data in Table 4 are generally consistent with crystallographic results, with EPR providing a systematically higher value for metal−metal and interplanar separations owing presumably to the absence of crystal packing effects and $\pi-\pi$ stacking in frozen solution.[23]

Spectroscopic Comparison. The absorption and emission properties of **1** and **5** and their zinc, copper, and nickel complexes are consistent with the structural geometries observed in the solid state and in solution. Electronic absorption and emission data for **1**−**8** are collected in Tables 5 and 6, respectively. Soret (B) and Q absorption bands arising from the standard four-orbital model for porphyrin spectra[26] undergo varying degrees of perturbation upon cofacially disposing two porphyrin rings using xanthene or dibenzofuran. The spectra of the biszinc(II) derivatives **2** and **6**, shown in Figure 5, are exemplary of each series. Figure 5a compares the electronic absorption spectra of Zn_2(DPX) (**2**), Zn_2(DPD) (**6**), and their monomer analog Zn(Etio-I) (Etio-I = etioporphyrin-I) in dichloromethane solution.

Table 5. UV−Visible Absorption Data for DPX and DPD Complexes in Dichloromethane at 298 K, λ_{abs}/nm (ϵ/1000 M^{-1} cm^{-1})[a]

	Soret (B)		Q region		
H_4(DPX) (**1**)	382 (202)	509 (11.6)	541 (6.4)	578 (7)	631 (2.9)
Zn_2(DPX) (**2**)	389 (290)	541 (14.3)		576 (13.2)	
Cu_2(DPX) (**3**)	387 (265)	534 (16.7)		571 (19.8)	
Ni_2(DPX) (**4**)	388 (305)	526 (13.6)		564 (23)	
H_4(DPD) (**5**)	397 (276)	501 (25)	536 (13.5)	571 (11.8)	625 (5.2)
Zn_2(DPD) (**6**)	400 (512)	534 (30.6)		571 (29.6)	
Cu_2(DPD) (**7**)	397 (400)	528 (17.6)		565 (23.4)	
Ni_2(DPD) (**8**)	395 (411)	521 (20.6)		560 (39.4)	

[a] Extinction coefficients (ϵ) are reported for the cofacial bisporphyrin unit.

Table 6. Singlet Excited State Parameters for DPX and DPD Complexes in Dichloromethane Solution at 298 K

	λ_{em} (nm)[a]	Φ_{fl}[b]	τ_{fl} (ns)[c]
H_4(DPX) (**1**)	637, 671, 703	0.0298 ± 0.009	10.55 ± 0.01
Zn_2(DPX) (**2**)	591, 640	0.0084 ± 0.001	1.35 ± 0.01
H_4(DPD) (**5**)	628, 658, 694	0.0870 ± 0.010	10.70 ± 0.10
Zn_2(DPD) (**6**)	578, 631	0.0541 ± 0.001	1.50 ± 0.02
H_2(Etio-I)	623, 649, 674, 689	0.1200 ± 0.008	11.50 ± 0.10
Zn(Etio-I)	572, 625	0.0298 ± 0.009	1.45 ± 0.01

[a] λ_{em} is the corrected emission fluorescence energy maximum. [b] Φ_{fl} is the quantum yield for emission fluorescence. [c] τ_{fl} is the observed fluorescence lifetime.

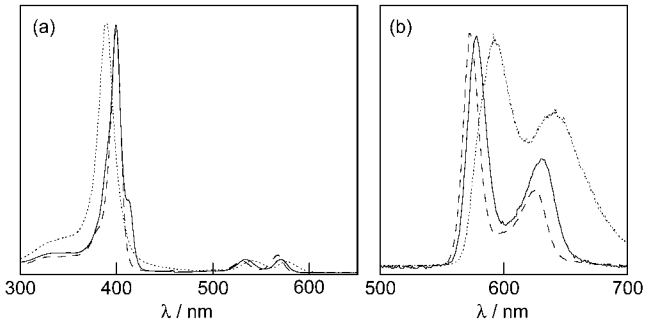

Figure 5. (a) Absorption and (b) emission spectra of Zn_2(DPX) (**2**) (dotted line), Zn_2(DPD) (**6**) (solid line), and Zn(Etio-I) (dashed line) in dichloromethane solution at room temperature. Spectra are normalized in intensities.

Characteristic of strongly interacting porphyrin subunits,[27,28] the B band of Zn_2(DPX) (**2**) is blue-shifted ($\lambda_{abs} = 389$ nm, $\epsilon = 290\,000$ M^{-1} cm^{-1}) and broadened relative to that of both Zn_2(DPD) (**6**) ($\lambda_{abs} = 400$ nm, $\epsilon = 512\,000$ M^{-1} cm^{-1}) and the monomer ($\lambda_{abs} = 400$ nm, $\epsilon = 200\,000$ M^{-1} cm^{-1}), while the Q(1,0) ($\lambda_{abs} = 541$ nm, $\epsilon = 14\,300$ M^{-1} cm^{-1}) and Q(0,0) ($\lambda_{abs} = 576$ nm, $\epsilon = 13\,200$ M^{-1} cm^{-1}) maxima are shifted to the red [$\lambda_{abs} = 534$ and 571 nm for **6**, 529 and 567 nm for Zn(Etio-I)]. In contrast, the absorption characteristics of Zn_2(DPD) (**6**) more closely approximate the monomer. The observed spectral differences are consistent with the enlarged distance between the two porphyrin chromophores imparted by the dibenzofuran backbone of DPD. The increased separation decreases $\pi-\pi$ overlap and exciton coupling between the porphyrin subunits. Similar trends are observed for DPA and DPB, where the exciton coupling in the latter series is greater due to its more compressed cofacial structure.[1] Both **2** and **6** produce strong

(25) Eaton, S. S.; Eaton, G. R.; Chang, C. K. *J. Am. Chem. Soc.* **1985**, *107*, 3177−3184.
(26) Gouterman, M. *J. Mol. Spectrosc.* **1961**, *6*, 138−163.
(27) Gouterman, M.; Holten, D.; Lieberman, E. *Chem. Phys.* **1977**, *25*, 139−153.
(28) Chang, C. K. *J. Het. Chem.* **1977**, *14*, 1285−1288.

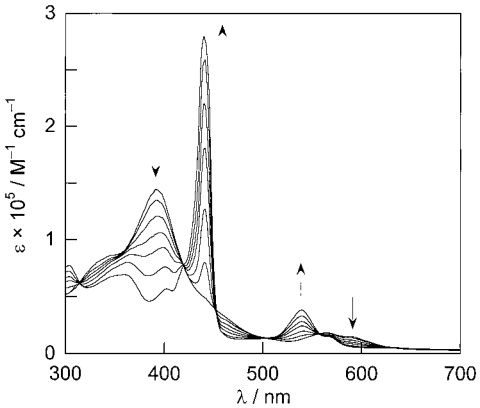

Figure 6. The absorption profiles demonstrate the conversion of benzene solutions of $Fe_2O(DPD)$ **10** (ca. 10^{-6} M) in the presence of triethyl phosphite ($P(OEt)_3$, ca. 0.2 M) at 298 K. The arrows indicate the disappearance of **10** and the appearance of $Fe_2(DPD)(P(OEt)_3)_2$. Spectra were recorded over the span of 2 h.

fluorescence typical of Q(0,0) and Q(1,0) excitation. As with the Q-band profile, a correspondent red-shift of these emission bands relative to monomer is observed for **2** (λ_{em} = 589 and 640 nm for **2**, λ_{em} = 572 and 625 nm for monomer), while **6** (λ_{em} = 578 and 631 nm) is similar to the monomer (Figure 5b). In addition, the shortened singlet excited-state lifetime (τ_{fl} = 1.35 ± 0.01 ns) and reduced quantum yield (Φ_{fl} = 0.0084 ± 0.001) of **2** compared to **6** (τ_{fl} = 1.50 ± 0.02 ns, Φ_{fl} = 0.0541 ± 0.001) provide more evidence that exciton coupling is greater in the former. The free-base porphyrins **1** and **5** also exhibit fluorescence that follow the trend of their biszinc(II) congeners. Compounds **1** and **5** show a phyllo-type splitting pattern that is known for mono-*meso*-substituted free-base porphyrins, with the intensity of the Q-bands displaying the following pattern: $Q_y(1,0) > Q_y(0,0) > Q_x(1,0) > Q_x(0,0)$. The spectra of the homobimetallic copper(II) and nickel(II) derivatives are of the hypso type, due to the overlap between the filled d_{xz} and d_{yz} orbitals and the empty porphyrin π^* levels. The relative energies of the Q-bands of the DPX and DPD derivatives follow the trend biszinc(II) > biscopper(II) > bisnickel(II), which is expected from Gouterman's four-orbital model analysis.[26]

Reactivity Comparison. The reactivity consequences arising from the structural and spectroscopic results collected for the DPX and DPD systems are manifested in the photoinduced oxidation of phosphite substrates by the bisiron(III) μ-oxo derivatives **9** and **10**, respectively. We note that this is a new mode of multielectron reactivity for the cofacial bisporphyrin motif. An exemplary substrate is triethyl phosphite, $P(OEt)_3$. Porphyrins **9** and **10** are thermally inert to $P(OEt)_3$; however, irradiation into the O−Fe LMCT transition of **9** and **10** at λ_{exc} > 365 nm in the presence of excess phosphite in benzene solution under anaerobic conditions leads to changes in their absorption spectra. Figure 6 shows the evolution of the absorption profiles for the photolysis of **10** under such conditions. Complex **9** behaves similarly under these photochemical conditions. A clean and quantitative photoreaction is evidenced by well-anchored isosbestic points, which are maintained throughout the irradiation. With the appearance of the final absorption spectrum, no additional changes are observed with continued irradiation. In addition, no spectral changes are observed upon irradiation in the absence of phosphite or porphyrin. For both photolysis reactions, a single porphyrin product is isolated with electronic absorption spectra identical to those of independently prepared iron(II) porphyrin complexes containing axial phosphite ligands;[29] the spectra are consistent with five-coordinate iron(II) porphyrins. We therefore assume that each iron is coordinated by a phosphite ligand, though we do not have direct evidence for distinguishing between ligand binding inside and outside of the pocket. Moreover, each photoreaction yields a stoichiometric amount of O=$P(OEt)_3$, as determined by ^{31}P NMR. The results establish the following overall reaction sequence for the photoinduced oxygenation of phosphite by the bisiron(III) μ-oxo porphyrins **9** and **10**,

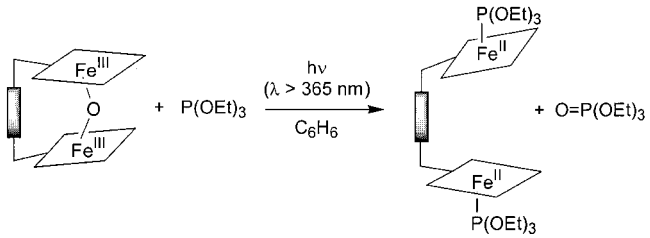

where the phosphites are shown to bind externally to the cofacial cleft. The efficiencies for the stoichiometric oxygen-atom abstraction reactions, reflected in the product appearance quantum yields (Φ_p), are markedly affected by the choice of spacer. For example, photoreaction of DPD complex **10** with a sterically modest phosphite such as trimethyl phosphite, $P(OMe)_3$, proceeds with a Φ_p value of $7.4(7) \times 10^{-4}$, which is within the range of efficiency found for the photooxidation of substrates by bisiron(III) μ-oxo porphyrins with no bridging spacer.[30−32] In contrast, the analogous reaction with DPX complex **9** ($\Phi_p = 9.0(1) \times 10^{-8}$) is less efficient by a factor of ca. 4 orders of magnitude.

A systematic set of electronically homologous phosphite substrates spanning a wide range of steric demands was screened for their photochemical reactivity with **9** and **10**. The quantum yield data are collected in Table 7. The results follow the expected trend of decreased photochemical efficiency with increasing steric bulk of the substrate. Notably, sterically demanding phosphites such as $P(O^iPr)_3$ (^{i}Pr = isopropyl) and $P(OTMS)_3$ (TMS = trimethylsilyl) react with DPD complex **10** but not with DPX complex **9**. The transfer of oxo from the porphyrin platform is preferred for the side-on approach of substrate.[33] The trend in Table 7 is therefore consistent with the contention that substrate attack

(29) Iron(II) porphyrin complexes were independently prepared by reduction of the corresponding chloroiron(III) complexes with 0.5% Na/Hg amalgam in the presence of 0.2 M phosphite. For a compilation of phosphine and phosphite cone angles, see: Tolman, C. A. *Chem. Rev.* **1977**, *77*, 313−348.
(30) Peterson, M. W.; Rivers, D. S.; Richman, R. M. *J. Am. Chem. Soc.* **1985**, *107*, 2907−2915.
(31) Weber, L.; Hommel, R.; Behling, J.; Haufe, G.; Hennig, H. *J. Am. Chem. Soc.* **1994**, *116*, 2400−2408.
(32) Hennig, H.; Luppa, D. *J. Prakt. Chem.* **1999**, *341*, 757−767.

Table 7. Product Quantum Yields (Φ_p) for the Photoinduced Oxidation of Phosphites by Fe_2O(DPX) (**9**) and Fe_2O(DPD) (**10**) in Benzene Solution at 298 K[a]

	cone angle[b] (deg)	Φ_p	
		9	**10**
$P(OMe)_3$	107	$9.0(1) \times 10^{-8}$	$7.4(7) \times 10^{-4}$
$P(OEt)_3$	109	$5.0(1) \times 10^{-8}$	$3.2(4) \times 10^{-4}$
$P(O^iPr)_3$	130	no reaction	$2.2(2) \times 10^{-5}$
$P(OTMS)_3$	>172	no reaction	$2.2(3) \times 10^{-6}$

[a] The quantum yield experiments were performed in the presence of 0.2 M phosphite under anaerobic conditions. [b] Phosphite cone angles were obtained from the literature (ref 32). The cone angle for $P(OTMS)_3$ was estimated from the data reported for $P(O^tBu)_3$.

from the electronically favored side-on geometry is governed by the steric bulk of the phosphite substrate to hinder the abstraction of an oxygen atom from the cleft of the Pacman scaffold.

Concluding Remarks

The multielectron reactivity of pillared cofacial bisporphyrins toward small-molecule substrates is predicated on the ability of the spacer to provide a bimetallic cleft of proper size and flexibility to efficiently accommodate reaction intermediates during catalysis.[1] Traditional systems based on anthracene (DPA) and biphenylene (DPB) exhibit notable activity, but their restrictions in vertical pocket size variability (ca. 1 Å) limit their use for systematic explorations of structure−activity relationships pertaining to the Pacman effect. In contrast, crystallographic analysis confirms the ability of the DPX and DPD platforms to provide cofacial pockets with an array of vertical sizes that can be tuned by axial ligation and/or metal substitution. Especially noteworthy is the ability of the DPD system to span a vertical range of metal−metal distances of over 4 Å. The structural studies are supported by EPR spectroscopy of the biscopper(II) derivatives, which directly probe metal−metal interactions in frozen solution. In addition, steady-state and time-resolved absorption and emission experiments reveal the general trend that the more compressed DPX complexes exhibit a greater degree of exciton coupling compared to their splayed DPD counterparts in fluid solution.

The chemical consequences of the structural and spectroscopic data collected for DPX and DPD are reflected in their multielectron reactivity. Previous studies have shown that biscobalt(II) complexes of both DPX and DPD are catalysts for the selective four-electron, four-proton reduction of oxygen to water, demonstrating that scaffolds with directed vertical flexibility (DPD) can yield comparable cooperative activity to preorganized clefts (DPX).[22] We show here that vertical ligand flexibility is also important for the multielectron photooxidation chemistry of cofacial bisporphyrin systems. The superior photoreactivity (ca. 10 000-fold) of the bisiron(III) μ-oxo DPD complex to oxidize phosphites is ascribed to the enhanced vertical range and flexibility that the dibenzofuran spacer provides for this cofacial platform. The data suggest that the bisiron(III) μ-oxo complex of the DPD framework is, in a structural sense, "spring-loaded",[34] and cleavage of the Fe—O bond with a photon presents an active species for efficient side-on oxygen abstraction by substrate. In closing, our results show that the DPX and DPD systems afford a unique combination of synthetic availability and vertical flexibility and that these attributes have implications for multielectron reactivity. Future studies of these and related platforms[15,35−37] for the catalytic transformation of small-molecule substrates should prove intriguing.

Acknowledgment. C.J.C. kindly thanks the National Science Foundation and the MIT/Merck Foundation for predoctoral fellowships. E.A.B. is grateful to NSERC (Canada) for a postgraduate scholarship. We thank Y. Oda for enlightening discussions. This work was supported by the National Science Foundation (CHE-0132680) and National Institutes of Health (GM 47274).

Supporting Information Available: An X-ray crystallographic file, in CIF format. This material is available free of charge via the Internet at http://pubs.acs.org.

IC0111029

(33) Groves, J. T.; Myers, R. S. *J. Am. Chem. Soc.* **1983**, *107*, 5791−5796.

(34) Pistorio, B. J.; Chang, C. J.; Nocera, D. G. *J. Am. Chem. Soc.*, in press.

(35) Chang, C. J.; Yeh, C.-Y.; Nocera, D. G. *J. Org. Chem.* **2002**, *67*, 1403−1406.

(36) Chang, C. J.; Deng, Y.; Peng, S.-M.; Lee, G.-H.; Yeh, C.-Y.; Nocera, D. G. *Inorg. Chem.* **2002**, in press.

(37) Yeh, C.-Y.; Chang, C. J.; Nocera, D. G. *J. Am. Chem. Soc.* **2001**, *123*, 1513−1514.